Prevalence of Two-Dimensional Photonic Topology

Ali Ghorashi,[1,*] Sachin Vaidya,[1,2] Mikael C. Rechtsman,[2] Wladimir A. Benalcazar,[3] Marin Soljačić,[1] and Thomas Christensen[1,4,†]

[1]Department of Physics, Massachusetts Institute of Technology, Cambridge, Massachusetts 02139, USA
[2]Department of Physics, The Pennsylvania State University, University Park, Pennsylvania 16801, USA
[3]Department of Physics, Emory University, Atlanta, Georgia 30322, USA
[4]Department of Electrical and Photonics Engineering, Technical University of Denmark, 2800 Kgs. Lyngby, Denmark

(Received 10 October 2023; accepted 24 June 2024; published 2 August 2024)

Despite intense research in topological photonics for more than a decade, the basic question of whether photonic band topology is rare or abundant—i.e., its relative prevalence—remains open. Here, we use symmetry analysis and a dataset of 550 000 synthetic two-dimensional photonic crystals to determine the prevalence of stable, fragile, and higher-order topology across 11 plane groups and find a general abundance of nontrivial band topology. Below the first band gap and with time-reversal symmetry, stable topology is more prevalent in the transverse electric polarization, is weakly dependent on contrast, and fragile topology is nearly absent. In time-reversal broken settings, Chern insulating phases are also abundant, albeit less so in threefold symmetric settings. Our results elucidate the role of symmetry, dielectric contrast, polarization, and time-reversal breaking in engendering topological photonic phases and may inform new design principles for their experimental realization.

DOI: 10.1103/PhysRevLett.133.056602

Topological properties of photonic crystals (PhCs) [1,2] have attracted substantial interest since the prediction of topological insulators in electronic systems [3,4]. Recent research has run the gamut of time-reversal (T) invariant and broken topology, ranging across topological degeneracies [5], Chern phases [6–9], higher-order topology [10,11], and beyond. Here, we investigate the prevalence of stable, fragile, and higher-order photonic topology in all two-dimensional (2D) symmetry settings that admit their symmetry-based identification. In this pursuit, we create a database of topological 2D PhCs, analogous to recent databases of electronic and phononic materials [12–17].

Our Letter is motivated by the following questions: How prevalent is nontrivial photonic topology? How is this prevalence affected by dielectric contrast, symmetries, and mode polarization? Are certain regions of the photonic band structure more likely to be topological than others? Answering these questions is of fundamental importance for the understanding, design, and experimental realization of photonic topological phenomena, because an understanding of the parameter space of topology can inform general design principles—e.g., the symmetries, geometric features, and dielectric contrasts most advantageous to engendering topological phases. To address these questions, we adopt recent symmetry-based topological frameworks [18–22], that have recently seen application and adaptation also to the photonic context [23–29]. Their generality and efficiency naturally lend them to high-throughput calculations, enabling us to answer the above questions by comprehensively sampling the design space of 2D PhCs.

Methodology—We briefly summarize the symmetry-based approach, which diagnoses topology from the ability to decompose a set of bands into linear combinations of elementary band representations (EBRs) [30,31]. These EBRs span the space of symmetry-respecting atomic limits (symmetric, exponentially localized Wannier orbitals). For example, in a mirror-symmetric 1D crystal (line group $p1m$) there are four EBRs, induced by placing even or odd Wannier orbitals at either the unit cell center or boundary. We restrict our focus to sets of bands that are $\mathbf{k}$-wise gapped from all other bands along all high-symmetry $\mathbf{k}$ lines (i.e., satisfy compatibility relations [32]), and call such sets "multiplets." Conceptually, if such a multiplet cannot be expressed as a sum (physically, a "stack") of EBRs, there is a topological obstruction to smoothly deforming the multiplet to an atomic limit. More technically, given a trivial multiplet $\mathfrak{n}$ in a PhC with plane group symmetry G, $\mathbf{k}$-wise gapped from all other bands, there exists a symmetry- and gap-preserving equivalence relation between $\mathfrak{n}$ and a decomposition in the EBRs of G [19–21]:

$$\mathfrak{n} \sim \bigoplus_{\mathbf{q}\alpha} m^{\alpha}_{\mathbf{q}} (\mathbf{q}|D^{\alpha}_{\mathbf{q}}). \tag{1}$$

Here, $(\mathbf{q}|D^{\alpha}_{\mathbf{q}})$ denotes an EBR induced from a maximal Wyckoff position $\mathbf{q}$ in G, transforming like the αth irre-

*Contact author: aligho@mit.edu
†Contact author: thomas@dtu.dk

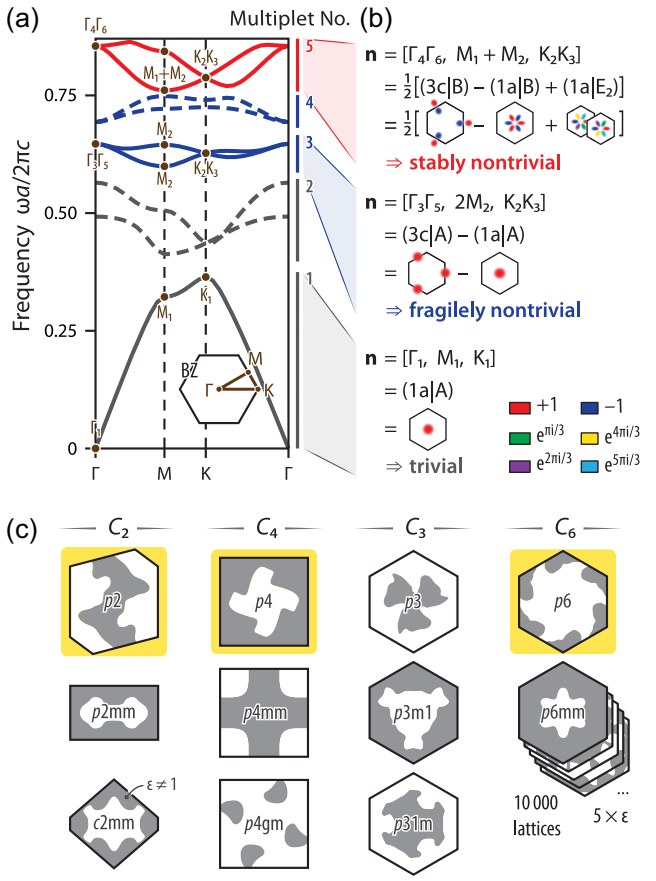

FIG. 1. Methodology, workflow, and dataset. (a) Band structure of a *p6*-symmetric PhC, hosting five separable bands, i.e., multiplets [TE polarization, unit cell from (c)]. (b) For each multiplet, we decompose the symmetry vectors, $\mathbf{n}$, in EBRs to obtain a symmetry-based diagnosis of band topology from the decomposition's coefficients. (c) Examples of PhC unit cells in our dataset, spanning 11 plane groups, each labeled in Hermann–Mauguin notation [63] and grouped by their rotational symmetry (C_n). Groups that admit stable, T-invariant topology are highlighted in yellow.

ducible representation (irrep) $D^\alpha_{\mathbf{q}}$ of the associated site-symmetry group $G_{\mathbf{q}} \equiv \{g \in G | g\mathbf{q} = \mathbf{q}\}$, and $m^\alpha_{\mathbf{q}} \in \{0, 1, 2, \ldots\}$ is the decomposition's EBR multiplicity.

The key simplification of symmetry-based frameworks [19–21] is to relax the strict functional decomposition of Eq. (1) to a decomposition of band symmetries. Specifically, we decompose the so-called symmetry vector $\mathbf{n}$ of $\mathfrak{n}$—enumerating the symmetry content of $\mathfrak{n}$ through the multiplicities $n^\alpha_{\mathbf{k}}$ of little group irreps $D^\alpha_{\mathbf{k}}$ across all high-symmetry $\mathbf{k}$ points—into the symmetry vectors $\mathbf{n}_{(\mathbf{q}|D^\alpha_{\mathbf{q}})}$ associated with each EBR $(\mathbf{q}|D^\alpha_{\mathbf{q}})$:

$$\mathbf{n} = \sum_{\mathbf{q}\alpha} c^\alpha_{\mathbf{q}} \mathbf{n}_{(\mathbf{q}|D^\alpha_{\mathbf{q}})}. \tag{2}$$

The symmetry-inferable topological diagnosis is made on the basis of the decomposition coefficients $c^\alpha_{\mathbf{q}}$ [21,33,34] [Figs. 1(a) and 1(b)]: if all $c^\alpha_{\mathbf{q}}$ can be chosen as non-negative integers, $\mathfrak{n}$ is compatible with the symmetries of an atomic limit, i.e., nominally topologically trivial [35]. If the decomposition must include EBRs that are not centered at the unit cell origin, $\mathfrak{n}$ is also said to be an obstructed atomic limit, which may host bulk polarization and corner anomalies with corresponding filling anomalies [26]. Conversely, if a decomposition exists with integer $c^\alpha_{\mathbf{q}}$ but requiring at least one negative coefficient, $\mathfrak{n}$ is topologically fragile [37]: by addition of appropriate atomic limits (namely, the EBRs associated with negative $c^\alpha_{\mathbf{q}}$), the band topology is trivial. In contrast, if the decomposition requires non-integer, rational $c^\alpha_{\mathbf{q}}$, the topology of $\mathfrak{n}$ is stably nontrivial [18]—being trivializable only by other nontrivial bands. If no decomposition exists, $\mathbf{n}$ describes a set of band symmetries that are inconsistent with compatibility relations [32], indicating a set of bands that is not gapped along high-symmetry $\mathbf{k}$ lines. We implemented a software package, MPBUTILS.JL [38], to facilitate this analysis, allowing automatic clustering and diagnosis of compatibility-respecting photonic bands [39]. The Supplemental Material [40], S1 and S2, provides a technical glossary and further methodological details.

PhC dataset—Of the 17 plane groups that describe the symmetry settings of 2D PhCs, only 11 allow symmetry-based distinctions between trivial and fragile or stable topology [21,34], namely those with a proper subgroup of $C_{n\geq 2}$. For each of these 11 plane groups, we generated 10 000 random PhC unit cells using a Fourier-based level-set technique [24,64] [Fig. 1(c) and the Supplemental Material [40], S11). Summarizing, we consider a "two-tone" dielectric motif in each unit cell: in one region, Ω_1, we place vacuum and in the other, Ω_ε, a dielectric with permittivity ε, scanning parametrically across $\varepsilon \in \{8, 12, 16, 24, 32\}$ and sampling filling fractions $|\Omega_\varepsilon|/(|\Omega_\varepsilon| + |\Omega_1|)$ randomly from a uniform distribution between 0.2 and 0.8. We remark that the topological prevalence in permeability-defined PhCs is one-to-one related to the prevalence in permittivity-defined PhCs due to electromagnetic duality (Supplemental Material [40], S8). For each PhC, we compute the requisite band symmetries at high-symmetry $\mathbf{k}$ points for the first 40 bands, using MIT PHOTONIC BANDS [65] and the tooling developed in Ref. [24], for both transverse electric (TE) and magnetic (TM) polarizations, obtaining the corresponding symmetry vectors of each separable multiplet [Figs. 2(a) and 2(b)]. Finally, each multiplet's symmetry-diagnosable band topology is determined via Eq. (2). Altogether, our dataset encompasses 11 (symmetry) × 10 000 (motif) × 5 (contrast) × 2 (polarization) = 1 100 000 distinct calculations. We use a 64 × 64 discretization grid and include 40 bands (convergence analysis in the Supplemental Material [40], S15), for which a typical single-core calculation (Xeon Platinum 8260) takes on the order of 20 s.

Stable and fragile topology—Figure 2 summarizes our results on the prevalence of stable and fragile topology in T-invariant 2D PhCs. We report the prevalence of band topology multiplet by multiplet rather than cumulatively

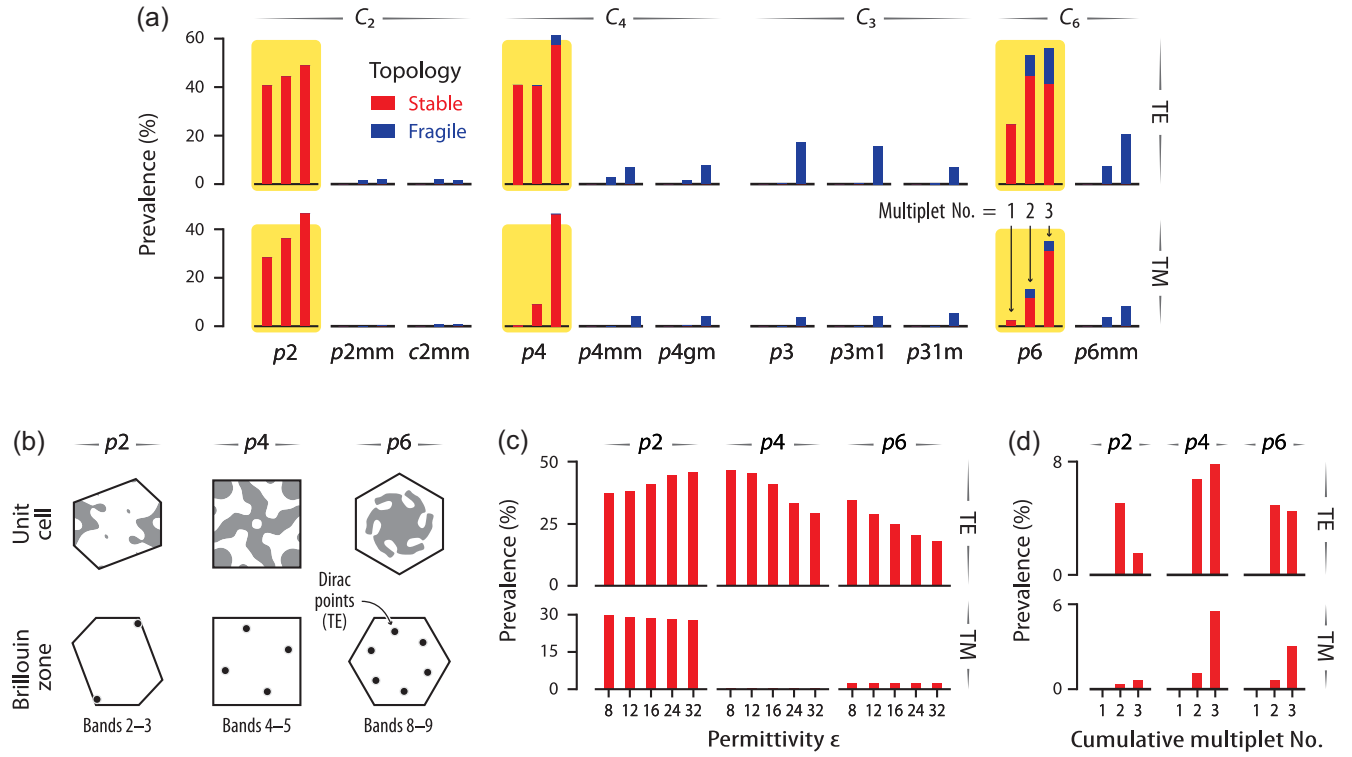

FIG. 2. Prevalence of stable and fragile time-reversal invariant topology. (a) Prevalence of symmetry-identifiable stable and fragile topology across plane groups (permittivity $\varepsilon = 16$; prevalence reported multiplet by multiplet). Plane groups that allow symmetry-based identification of stable topology are highlighted in yellow. (b) Examples of three PhCs with stable topology and associated Dirac points at generic $\mathbf{k}$ points (TE polarization). The selected examples have no intersecting trivial bulk "Fermi pockets," i.e., the Dirac points are frequency isolated. (c) Permittivity dependence of stable topology in *p2*, *p4*, and *p6* for the first multiplet. (d) Fraction of cumulatively stable multiplets whose associated Dirac points are frequency isolated. A nearly complete absence is observed in the first multiplet.

(i.e., up to and including the nth multiplet), because cumulative fragile topology is nearly absent (cumulative statistics in the Supplemental Material [40], S7).

We focus first on T-invariant stable topology, which is symmetry diagnosable in just three plane groups—*p2*, *p4*, and *p6* (i.e., with $C_{n=2,4,6}$-symmetric unit cells) [21]—and indicates an odd number of Dirac points in each n-fold symmetric Brillouin zone (BZ) sector (equivalently, a π Berry phase for loops encircling such sectors) [36,66], with associated edge states connecting their boundary projections (Supplemental Material [40], S9.B) [26,67,68]. Figure 2(a) summarizes our results for a fixed permittivity of $\varepsilon = 16$ for the dielectric region. Surprisingly, stable topology is widely prevalent. For example, given a random PhC in *p2*, one should expect Dirac points with a likelihood of ~30%–50%, depending on multiplet and polarization. We emphasize that these Dirac points are qualitatively different from the more familiar doublet of Dirac points at the BZ boundary ($\mathbf{K}$ and $\mathbf{K}'$ points) of C_6-symmetric settings [69,70]: here, instead, there are n mod $2n$ Dirac points in the BZ interior [Fig. 2(b)]. Polarization-wise, we find that stable topology is more prevalent in the TE than the TM polarization, especially evident in *p4* and *p6* where stable topology in the first TM multiplet is nearly absent. Further, varying the permittivity of the dielectric region [Fig. 2(c)], we observe that the overall prevalence is only weakly dependent on dielectric contrast: physically, dielectric contrast mainly controls the size of band gaps—affecting band symmetries and topology only if multiple band closures separate the band structure from the empty-lattice limit. As such, geometry is the main design variable for engendering stable PhC topology. The prevalence of frequency-isolated Dirac points—i.e., Dirac points whose frequency do not intersect other bulk bands—is a small fraction of the overall prevalence of stable topology, however [Fig. 2(d)]: nearly absent in the first multiplet and at most a few percent in higher multiplets. Of this small fraction, a still smaller fraction falls below the light line (Supplemental Material [40], S6.A).

Unlike stable topology, fragile topology is symmetry diagnosable in all 11 plane groups [Fig. 2(a)]. Although far less prevalent than its stable counterpart, several plane groups feature a substantial prevalence of fragile bands, especially among higher multiplets. We find fragile bands in settings with both C_2T and C_3 symmetry (characterized by relatively winding "straight" [18] and "concentric" [71,72] Wilson spectra, respectively). However, we find a nearly complete dearth of cumulatively fragile multiplets:

across our entire dataset, we identify just 43 PhCs with cumulatively fragile topology, all with centering-related EBR decompositions (Supplemental Material [40], S7). Despite recent progress [73–77], the observable consequences of cumulatively fragile topology remains largely an open question, especially in PhCs [23,78]. Analyzing the cumulatively fragile PhCs individually, we find that the corresponding bands feature *pairs* of nodal points in each n-fold symmetric BZ sector (Supplemental Material [40], S7).

Higher-order topology—Beyond the symmetry-indicated classifications of stable, fragile, and trivial (i.e., atomic limits) band topology [19–21] exists a finer gradation associated with higher-order topology and filling anomalies [79]. In particular, a filling anomaly exists in any finite C_n-symmetric tiling of a PhC unit cell with nonzero bulk polarization ($\mathbf{P}$) or corner anomaly (Q) associated with fractional mode densities at the tiling's edges or corners, respectively. Both $\mathbf{P}$ and Q can be evaluated from band symmetry [79]—or, equivalently, from the EBR decompositions of Eq. (2) (Supplemental Material [40], S5). We give values of $\mathbf{P}$ and Q in dimensionless units below; i.e., Q is defined modulo 1 and $\mathbf{P}$ modulo direct lattice vectors.

We restrict our attention to multiplets without cumulatively stable topology, i.e., integer EBR decomposition coefficients, corresponding to bands that are symmetry compatible with a gapped trivial or fragile limit. For each PhC sample, at a given unit-cell centering choice, we classify its multiplets as higher-order nontrivial if it has vanishing bulk polarization ($\mathbf{P} = \mathbf{0}$) and nonzero corner anomaly ($Q \neq 0$). By requiring $\mathbf{P} = \mathbf{0}$ we ensure that a $Q \neq 0$ filling anomaly is strictly isolated to corners, and not coexisting with a corresponding edge anomaly [26,79–82]; additionally, if $\mathbf{P} \neq \mathbf{0}$, the definition of Q is dependent on the tiling's boundary configuration in C_3-symmetric settings (Supplemental Material [40], S5.F). Unlike assignment of stable and fragile band topology, $\mathbf{P}$ and Q are generally dependent on the choice of unit-cell centering (Supplemental Material [40], S5.B). Because of this, when assessing higher-order topology, we augment our dataset to include all the possible recenterings of a C_n-symmetric PhC that preserves a C_n axis at the unit cell origin, treating each recentered PhC as a distinct sample.

Figure 3 reports the prevalence of higher-order topology consistent with this definition, along with supercell calculations of selected samples showcasing the associated corner anomaly. Prevalence is highest in plane groups with a C_6 subgroup, lowest in those with only a C_2 subgroup, and intermediate in those with a C_4 or C_3 maximal subgroup. In particular, we highlight two interesting features in specific plane groups. First, an absence of nontrivial higher-order topology is observed below the third multiplet in $p2$: this is because a $\{\mathbf{P} = \mathbf{0}, Q \neq 0\}$ multiplet requires three bands in C_2-symmetric settings, but

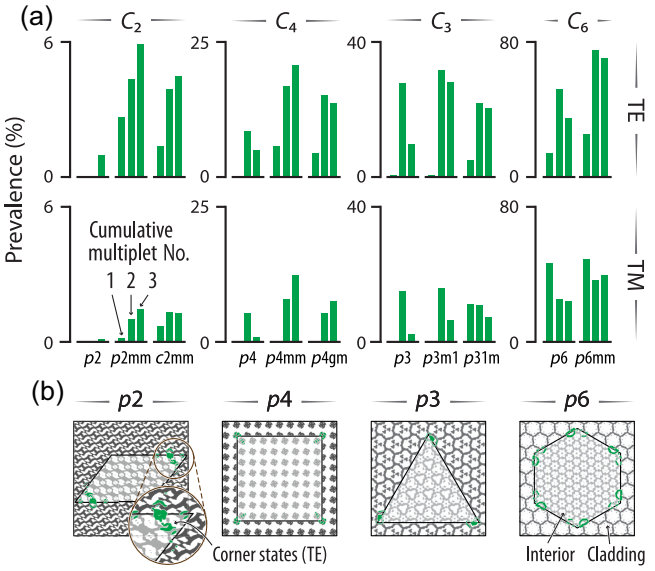

FIG. 3. Prevalence of corner anomalies. (a) Prevalence of cumulative higher-order topology, as defined in the main text. (b) Supercell simulations of selected PhC samples with corner anomalies, clad by suitable atomic-limit PhCs (Supplemental Material [40], S5.E), in $p2$, $p4$, $p3$, and $p6$. Contours of energy density shown in green.

all $p2$ multiplets are singly degenerate (see the Supplemental Material [40], Sec. S5.D). Second, in plane groups $p31m$, $p6$, and $p6mm$, there always exists a centering choice that ensures $\mathbf{P} = \mathbf{0}$ (Supplemental Material [40], S5.G). Considering this, it is natural to expect a higher prevalence of higher-order topology in these settings. However, $p31m$ defies this expectation, suggesting that the prevalence of higher-order topology in $p6$ and $p6mm$ is attributable to their higher rotational symmetry.

Time-reversal breaking and Chern topology—Thus far, we have focused on T-invariant PhCs, which necessarily have trivial Chern topology. To assess the prevalence of nontrivial Chern phases under T breaking, and focusing on the TE polarization [83], we incorporate a gyroelectric effect due to a $\hat{\mathbf{z}}$-oriented external magnetic field. This lifts the scalar permittivity ε to an anisotropic, nonreciprocal tensor $\boldsymbol{\varepsilon}$ with off-diagonal and diagonal elements $\varepsilon_{xy} = -\varepsilon_{yx} = i\varepsilon B$ and $\varepsilon_{xx} = \varepsilon_{yy} = \varepsilon(1 + B^2)^{1/2}$, respectively, where B represents the effective magnetic field amplitude [5].

Fixing $\varepsilon = 16$ and restricting our attention to the C_n-symmetric plane groups—$p2$, $p4$, $p3$, and $p6$—that admit a symmetry-based identification of the Chern number modulo n [36], we report the prevalence of nonzero Chern numbers in Fig. 4. For the first multiplet, the results can be understood (and approximately lower-bounded for small B), from the corresponding prevalence of Dirac points under T symmetry [Fig. 4(a), red bars]. Specifically, in 2D, the sources of Chern topology are Dirac [6] and quadratic degeneracies [85]. In $p2$, for example, the only such sources are Dirac points in the BZ interior: as a result,

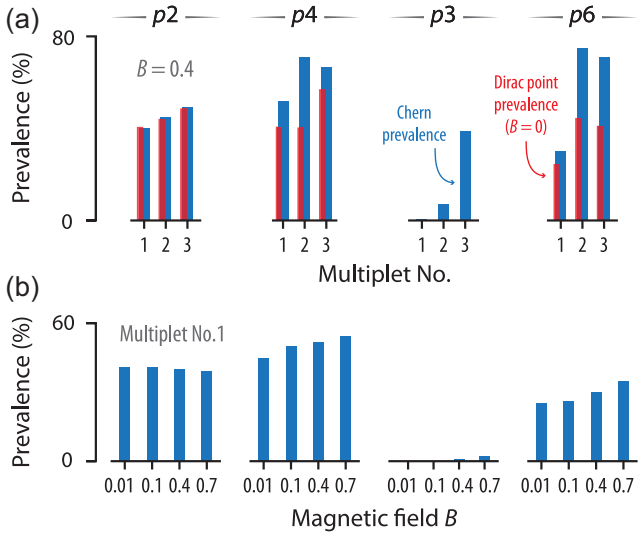

FIG. 4. Prevalence of Chern topology under time-reversal breaking. (a) Prevalence of nontrivial Chern topology in the lowest three multiplets an effective magnetic field $B = 0.4$ for TE polarization in plane groups *p2*, *p3*, *p4* and *p6*. (b) Prevalence of nontrivial Chern topology in the first multiplet as a function of magnetic field. Prevalence is reported multiplet by multiplet.

the prevalence of symmetry-identifiable stable T-invariant and T-broken nontrivial topology agrees exactly at small B. Conversely, *p4* and *p6* also allow T-protected Dirac and quadratic degeneracies at high-symmetry $\mathbf{k}$ points, contributing to a higher prevalence of Chern-nontrivial phases than their T-invariant counterparts. In contrast, *p3* does not support robust Dirac points due to its lack of twofold rotation symmetry. Instead, it admits a solitary quadratic degeneracy associated with the $\Gamma_2\Gamma_3$ irrep, whose T breaking can realize nontrivial Chern topology. The first multiplet of *p3*, however, is singly degenerate and so never includes this irrep, which explains its associated absence of nonzero Chern numbers.

For larger magnetic fields [Fig. 4(b)], this simple understanding of breaking T-protected degeneracies is modified by the potential for driving multiple band inversions as B is increased. In the aggregate, however, the influence of T-breaking strength is modest since such inversions tend to produce changes of the band topology that average out over distinct PhC samples.

Discussion—By comprehensively sampling the space of symmetric 2D PhCs, we have investigated the relative abundance of stable, fragile, and higher-order photonic topology. Our Letter demonstrates that the prevalence of photonic topological band features is mainly affected by polarization, symmetry, and geometry—and only to a lesser extent by dielectric contrast and T-breaking amplitude, which mainly affect the spectral separation between bands. Contrary to the prevalent association of photonic topology with exotic or rare phenomena—but consistently with recent results from the electronic and phononic domains [12–17]—we conclude that photonic topology is very prevalent. Certain photonic topological features, most notably cumulatively fragile topology, remain rare, however.

Our Letter motivates investigations along several lines [86]. For instance, can we understand the observed statistics physically, e.g., via the empty-lattice approximation? What is the physical reason for the near absence of cumulative fragile topology? What are the most naturally observable consequences of fragile topology in photonics? Does a similar abundance exist for 3D PhCs? And, within a particular symmetry setting, which geometrical motifs are most associated with topological band features? Our dataset [93] may also enable machine-learning-based investigations into topological physics [88,89] and photonics [64,90,91]. Finally, the prevalence observed in our Letter highlights that the main design challenge of photonic topology is one of finding desired band topology *jointly* with desired spectral properties, e.g., large topological gaps or well-isolated degeneracies, motivating further research in topological inverse design [25,92].

Acknowledgments—A. G. acknowledges the support of the National Science Foundation Graduate Research Fellowship (GRFP). W. A. B. acknowledges start-up funds from Emory University. T. C. acknowledges the support of a research grant (Project No. 42106) from Villum Fonden and an insightful suggestion from Andrei Laurynenka on duality. This research is based upon work supported in part by the Air Force Office of Scientific Research under Grants No. FA9550-20-1-0115 and No. FA9550-21-1-0299, the U.S. Office of Naval Research (ONR) Multidisciplinary University Research Initiative (MURI) Grant No. N00014-20-1-2325 on Robust Photonic Materials with High-Order Topological Protection, and the U.S. Army Research Office through the Institute for Soldier Nanotechnologies at MIT under Collaborative Agreement No. W911NF-23-2-0121. The MIT SuperCloud and Lincoln Laboratory Supercomputing Center provided computing resources that contributed to the results reported in this work.

Data availability—The supporting data for this Letter are openly available from [93].

[1] L. Lu, J. D. Joannopoulos, and M. Soljačić, Topological photonics, Nat. Photonics **8**, 821 (2014).
[2] T. Ozawa, H. M. Price, A. Amo, N. Goldman, M. Hafezi, L. Lu, M. C. Rechtsman, D. Schuster, J. Simon, O. Zilberberg, and I. Carusotto, Topological photonics, Rev. Mod. Phys. **91**, 015006 (2019).
[3] L. Fu, C. L. Kane, and E. J. Mele, Topological insulators in three dimensions, Phys. Rev. Lett. **98**, 106803 (2007).
[4] C. L. Kane and E. J. Mele, Quantum spin Hall effect in graphene, Phys. Rev. Lett. **95**, 226801 (2005).

[5] L. Lu, L. Fu, J. D. Joannopoulos, and M. Soljačić, Weyl points and line nodes in gyroid photonic crystals, Nat. Photonics **7**, 294 (2013).

[6] F. D. M. Haldane and S. Raghu, Possible realization of directional optical waveguides in photonic crystals with broken time-reversal symmetry, Phys. Rev. Lett. **100**, 013904 (2008).

[7] Z. Wang, Y. Chong, J. D. Joannopoulos, and M. Soljačić, Observation of unidirectional backscattering-immune topological electromagnetic states, Nature (London) **461**, 772 (2009).

[8] S. A. Skirlo, L. Lu, Y. Igarashi, Q. Yan, J. Joannopoulos, and M. Soljačić, Experimental observation of large Chern numbers in photonic crystals, Phys. Rev. Lett. **115**, 253901 (2015).

[9] M. C. Rechtsman, J. M. Zeuner, Y. Plotnik, Y. Lumer, D. Podolsky, F. Dreisow, S. Nolte, M. Segev, and A. Szameit, Photonic Floquet topological insulators, Nature (London) **496**, 196 (2013).

[10] L. He, Z. Addison, E. J. Mele, and B. Zhen, Quadrupole topological photonic crystals, Nat. Commun. **11**, 3119 (2020).

[11] B.-Y. Xie, H.-F. Wang, H.-X. Wang, X.-Y. Zhu, J.-H. Jiang, M.-H. Lu, and Y.-F. Chen, Second-order photonic topological insulator with corner states, Phys. Rev. B **98**, 205147 (2018).

[12] T. Zhang, Y. Jiang, Z. Song, H. Huang, Y. He, Z. Fang, H. Weng, and C. Fang, Catalogue of topological electronic materials, Nature (London) **566**, 475 (2019).

[13] F. Tang, H. C. Po, A. Vishwanath, and X. Wan, Comprehensive search for topological materials using symmetry indicators, Nature (London) **566**, 486 (2019).

[14] M. Vergniory, L. Elcoro, C. Felser, N. Regnault, B. A. Bernevig, and Z. Wang, A complete catalogue of high-quality topological materials, Nature (London) **566**, 480 (2019).

[15] M. G. Vergniory, B. J. Wieder, L. Elcoro, S. S. P. Parkin, C. Felser, B. A. Bernevig, and N. Regnault, All topological bands of all nonmagnetic stoichiometric materials, Science **376**, eabg9094 (2022).

[16] J. Sødequist, U. Petralanda, and T. Olsen, Abundance of second order topology in C_3 symmetric two-dimensional insulators, 2D Mater. **10**, 015009 (2022).

[17] Y. Xu, M. G. Vergniory, D.-S. Ma, J. L. Mañes, Z.-D. Song, B. A. Bernevig, N. Regnault, and L. Elcoro, Catalogue of topological phonon materials, arXiv:2211.11776.

[18] J. Cano and B. Bradlyn, Band representations and topological quantum chemistry, Annu. Rev. Condens. Matter Phys. **12**, 225 (2021).

[19] B. Bradlyn, L. Elcoro, J. Cano, M. G. Vergniory, Z. Wang, C. Felser, M. I. Aroyo, and B. A. Bernevig, Topological quantum chemistry, Nature (London) **547**, 298 (2017).

[20] J. Kruthoff, J. de Boer, J. van Wezel, C. L. Kane, and R.-J. Slager, Topological classification of crystalline insulators through band structure combinatorics, Phys. Rev. X **7**, 041069 (2017).

[21] H. C. Po, A. Vishwanath, and H. Watanabe, Symmetry-based indicators of band topology in the 230 space groups, Nat. Commun. **8**, 50 (2017).

[22] H. C. Po, Symmetry indicators of band topology, J. Phys. Condens. Matter **32**, 263001 (2020).

[23] M. B. de Paz, M. G. Vergniory, D. Bercioux, A. García-Etxarri, and B. Bradlyn, Engineering fragile topology in photonic crystals: Topological quantum chemistry of light, Phys. Rev. Res. **1**, 032005(R) (2019).

[24] T. Christensen, H. C. Po, J. D. Joannopoulos, and M. Soljačić, Location and topology of the fundamental gap in photonic crystals, Phys. Rev. X **12**, 021066 (2022).

[25] S. Kim, T. Christensen, S. G. Johnson, and M. Soljačić, Automated discovery and optimization of 3D topological photonic crystals, ACS Photonics **10**, 861 (2023).

[26] S. Vaidya, A. Ghorashi, T. Christensen, M. C. Rechtsman, and W. A. Benalcazar, Topological phases of photonic crystals under crystalline symmetries, Phys. Rev. B **108**, 085116 (2023).

[27] S. Vaidya, M. C. Rechtsman, and W. A. Benalcazar, Polarization and weak topology in Chern insulators, Phys. Rev. Lett. **132**, 116602 (2024).

[28] A. Morales-Pérez, C. Devescovi, Y. Hwang, M. García-Díez, B. Bradlyn, J. L. Mañes, M. G. Vergniory, and A. García-Etxarri, Transversality-enforced tight-binding model for 3D photonic crystals aided by topological quantum chemistry, arXiv:2305.18257.

[29] C. Devescovi, A. Morales-Pérez, Y. Hwang, M. García-Díez, I. Robredo, J. L. Mañes, B. Bradlyn, A. García-Etxarri, and M. G. Vergniory, Axion topology in photonic crystal domain walls, arXiv:2305.19805.

[30] J. Zak, Band representations of space groups, Phys. Rev. B **26**, 3010 (1982).

[31] H. Bacry, L. Michel, and J. Zak, Symmetry and classification of energy bands in crystals, in *Group Theoretical Methods in Physics*, Lecture Notes in Physics (Springer, New York, 1988), pp. 289–308.

[32] L. P. Bouckaert, R. Smoluchowski, and E. Wigner, Theory of Brillouin zones and symmetry properties of wave functions in crystals, Phys. Rev. **50**, 58 (1936).

[33] L. Elcoro, Z. Song, and B. A. Bernevig, Application of induction procedure and Smith decomposition in calculation and topological classification of electronic band structures in the 230 space groups, Phys. Rev. B **102**, 035110 (2020).

[34] Z.-D. Song, L. Elcoro, Y.-F. Xu, N. Regnault, and B. A. Bernevig, Fragile phases as affine monoids: Classification and material examples, Phys. Rev. X **10**, 031001 (2020).

[35] While a non-negative integer decomposition in Eq. (1) strictly implies topological triviality, the same is not true for the decompositions in Eq. (2). Rather, such a decomposition only implies compatibility with the band symmetries of a trivial atomic limit, not necessarily trivial topology [21]: we call this "nominally trivial." For example, in T-broken C_n-symmetric PhCs, a "nominally trivial" diagnosis implies only that the Chern number vanishes modulo n [36]. However, the absence of a non-negative integer decomposition in Eq. (2) strictly implies nontrivial (stable or fragile) topology. Because of this, our symmetry-based assessments of topological prevalence in fact represent lower bounds.

[36] C. Fang, M. J. Gilbert, and B. A. Bernevig, Bulk topological invariants in noninteracting point group symmetric insulators, Phys. Rev. B **86**, 115112 (2012).

[37] H. C. Po, H. Watanabe, and A. Vishwanath, Fragile topology and Wannier obstructions, Phys. Rev. Lett. **121**, 126402 (2018).

[38] MPBUTILS.JL (v0.1.10), https://github.com/thchr/MPBUtils.jl (accessed 25 July, 2023).

[39] The 2D PhC problem is spared the complications of the Γ-point band-symmetry assignment issues of 3D PhCs [24]. Instead, the polarization of TE and TM modes imply a natural rule [23]: in the zero-frequency at Γ, the TM (TE) band transforms as a $\hat{\mathbf{z}}$-oriented vector (pseudovector).

[40] See Supplemental Material at http://link.aps.org/supplemental/10.1103/PhysRevLett.133.056602 which includes Refs. [41–62], for additional statistics, discussions, definitions, derivations, and results.

[41] C. J. Bradley and A. P. Cracknell, *The Mathematical Theory of Symmetry in Solids* (Clarendon Press, New York, 1972).

[42] G. de la Flor, B. Souvignier, G. Madariaga, and M. I. Aroyo, Layer groups: Brillouin-zone and crystallographic databases on the Bilbao Crystallographic Server, Acta Crystallogr. Sect. A **77**, 559 (2021).

[43] L. Elcoro, B. Bradlyn, Z. Wang, M. G. Vergniory, J. Cano, C. Felser, B. A. Bernevig, D. Orobengoa, G. de la Flor, and M. I. Aroyo, Double crystallographic groups and their representations on the Bilbao Crystallographic Server, J. Appl. Crystallogr. **50**, 1457 (2017).

[44] A. P. Cracknell, B. L. Davies, S. C. Miller, and W. F. Love, *Kronecker Product Tables. General Introduction and Tables of Irreducible Representations of Space Groups* (IFI/Plenum, New York, 1979), Vol. 1.

[45] Crystalline.jl (v0.4.21), https://github.com/thchr/Crystalline.jl (accessed 19 February, 2024).

[46] D. B. Litvin and T. R. Wike, *Character Tables and Compatibility Relations of the Eighty Layer Groups and Seventeen Plane Groups* (Springer, New York, NY, 1999).

[47] J. Cano, B. Bradlyn, Z. Wang, L. Elcoro, M. G. Vergniory, C. Felser, M. I. Aroyo, and B. A. Bernevig, Building blocks of topological quantum chemistry: Elementary band representations, Phys. Rev. B **97**, 035139 (2018).

[48] R. S. Mulliken, Report on notation for the spectra of polyatomic molecules, J. Chem. Phys. **23**, 1997 (1955).

[49] F. Tang, H. C. Po, A. Vishwanath, and X. Wan, Efficient topological materials discovery using symmetry indicators, Nat. Phys. **15**, 470 (2019).

[50] GNU Linear Programming Kit (GLPK), https://www.gnu.org/software/glpk.

[51] I. Dunning, J. Huchette, and M. Lubin, JuMP: A modeling language for mathematical optimization, SIAM Rev. **59**, 295 (2017).

[52] H. Watanabe and L. Lu, Space group theory of photonic bands, Phys. Rev. Lett. **121**, 263903 (2018).

[53] M. Blanco de Paz, C. Devescovi, G. Giedke, J. J. Saenz, M. G. Vergniory, B. Bradlyn, D. Bercioux, and A. GarcíaEtxarri, Tutorial: computing topological invariants in 2D photonic crystals, Adv. Quantum Technol. **3**, 1900117 (2019).

[54] M. Proctor, P. A. Huidobro, B. Bradlyn, M. B. de Paz, M. G. Vergniory, D. Bercioux, and A. García-Etxarri, Robustness of topological corner modes in photonic crystals, Phys. Rev. Res. **2**, 042038 (2020).

[55] *International Tables for Crystallography: Volume A*, edited by M. I. Aroyo, 7th ed. (International Union of Crystallography, 2016), 10.1107/9780955360206000114.

[56] M. C. Rechtsman, Y. Plotnik, J. M. Zeuner, D. Song, Z. Chen, A. Szameit, and M. Segev, Topological creation and destruction of edge states in photonic graphene, Phys. Rev. Lett. **111**, 103901 (2013).

[57] S. Y. Buhmann, D. T. Butcher, and S. Scheel, Macroscopic quantum electrodynamics in nonlocal and nonreciprocal media, New J. Phys. **14**, 083034 (2012).

[58] Q. Zhang, L. He, E. J. Mele, B. Zhen, and A. T. C. Johnson, General duality and magnet-free passive phononic Chern insulators, Nat. Commun. **14**, 916 (2023).

[59] J. D. Jackson, *Classical Electrodynamics*, 3rd ed. (John Wiley & Sons, New York, 1928).

[60] Y. Fang and J. Cano, Filling anomaly for general two- and three-dimensional C_4 symmetric lattices, Phys. Rev. B **103**, 165109 (2021).

[61] P. Bratley and B. L. Fox, Algorithm 659: Implementing Sobol's quasirandom sequence generator, ACM Trans. Math. Softw. **14**, 88 (1988).

[62] S. Joe and F. Y. Kuo, Remark on algorithm 659: Implementing Sobol's quasirandom sequence generator, ACM Trans. Math. Softw. **29**, 49 (2003).

[63] *International Tables for Crystallography Volume A: Space-Group Symmetry*, edited by M. I. Aroyo, 6th ed. (Wiley, New York, 2016).

[64] T. Christensen, C. Loh, S. Picek, D. Jakobović, L. Jing, S. Fisher, V. Ceperic, J. D. Joannopoulos, and M. Soljačić, Predictive and generative machine learning models for photonic crystals, Nanophotonics **9**, 4183 (2020).

[65] S. G. Johnson and J. D. Joannopoulos, Block-iterative frequency-domain methods for Maxwell's equations in a planewave basis, Opt. Express **8**, 173 (2001).

[66] Z. Song, T. Zhang, and C. Fang, Diagnosis for nonmagnetic topological semimetals in the absence of spin-orbital coupling, Phys. Rev. X **8**, 031069 (2018).

[67] P. Delplace, D. Ullmo, and G. Montambaux, Zak phase and the existence of edge states in graphene, Phys. Rev. B **84**, 195452 (2011).

[68] R. S. K. Mong and V. Shivamoggi, Edge states and the bulk-boundary correspondence in Dirac Hamiltonians, Phys. Rev. B **83**, 125109 (2011).

[69] G. W. Semenoff, Condensed-matter simulation of a three-dimensional anomaly, Phys. Rev. Lett. **53**, 2449 (1984).

[70] T. Ochiai and M. Onoda, Photonic analog of graphene model and its extension: Dirac cone, symmetry, and edge states, Phys. Rev. B **80**, 155103 (2009).

[71] B. Bradlyn, Z. Wang, J. Cano, and B. A. Bernevig, Disconnected elementary band representations, fragile topology, and Wilson loops as topological indices: An example on the triangular lattice, Phys. Rev. B **99**, 045140 (2019).

[72] J. G. B. Henke, Topology in crystals and symmetry-breaking from interactions, Ph.D. thesis, Institute for Theoretical Physics, University of Amsterdam, 2022.

[73] Y. Hwang, J. Ahn, and B.-J. Yang, Fragile topology protected by inversion symmetry: Diagnosis, bulk-boundary correspondence, and Wilson loop, Phys. Rev. B **100**, 205126 (2019).

[74] Z.-D. Song, L. Elcoro, and B. A. Bernevig, Twisted bulk-boundary correspondence of fragile topology, Science **367**, 794 (2020).
[75] V. Peri, Z.-D. Song, M. Serra-Garcia, P. Engeler, R. Queiroz, X. Huang, W. Deng, Z. Liu, B. A. Bernevig, and S. D. Huber, Experimental characterization of fragile topology in an acoustic metamaterial, Science **367**, 797 (2020).
[76] F. N. Ünal, A. Bouhon, and R.-J. Slager, Topological Euler class as a dynamical observable in optical lattices, Phys. Rev. Lett. **125**, 053601 (2020).
[77] G. F. Lange, A. Bouhon, and R.-J. Slager, Subdimensional topologies, indicators, and higher order boundary effects, Phys. Rev. B **103**, 195145 (2021).
[78] A. Alexandradinata, J. Höller, C. Wang, H. Cheng, and L. Lu, Crystallographic splitting theorem for band representations and fragile topological photonic crystals, Phys. Rev. B **102**, 115117 (2020).
[79] W. A. Benalcazar, T. Li, and T. L. Hughes, Quantization of fractional corner charge in C_n-symmetric higher-order topological crystalline insulators, Phys. Rev. B **99**, 245151 (2019).
[80] F. Schindler, M. Brzezińska, W. A. Benalcazar, M. Iraola, A. Bouhon, S. S. Tsirkin, M. G. Vergniory, and T. Neupert, Fractional corner charges in spin-orbit coupled crystals, Phys. Rev. Res. **1**, 033074 (2019).
[81] W. A. Benalcazar, B. A. Bernevig, and T. L. Hughes, Quantized electric multipole insulators, Science **357**, 61 (2017).
[82] W. A. Benalcazar, B. A. Bernevig, and T. L. Hughes, Electric multipole moments, topological multipole moment pumping, and chiral hinge states in crystalline insulators, Phys. Rev. B **96**, 245115 (2017).
[83] The TM modes are unaffected by the considered gyroelectric effect, since their **E** fields are $\hat{\mathbf{z}}$ oriented. An analogous gyromagnetic effect with nonreciprocal permeability, i.e., with $\mu_{xy} = -\mu_{yx} \neq 0$, breaks T for the TM polarized bands [7,84].
[84] Z. Wang, Y. D. Chong, J. D. Joannopoulos, and M. Soljačić, Reflection-free one-way edge modes in a gyromagnetic photonic crystal, Phys. Rev. Lett. **100**, 013905 (2008).
[85] Y. D. Chong, X.-G. Wen, and M. Soljačić, Effective theory of quadratic degeneracies, Phys. Rev. B **77**, 235125 (2008).
[86] As we were finalizing this manuscript, we became aware of related work under preparation [87].
[87] S. D. Huber, High-throughput generation of topological metamaterials, in *13th International Conference on Metamaterials, Photonic Crystals and Plasmonics, Paris, France* (2023), p. 781, https://www.rsc.org/events/detail/75111/meta-2023-the-13th-international-conference-on-metamaterials-photonic-crystals-and-plasmonics.
[88] A. Ma, Y. Zhang, T. Christensen, H. C. Po, L. Jing, L. Fu, and M. Soljačić, Topogivity: A machine-learned chemical rule for discovering topological materials, Nano Lett. **23**, 772 (2023).
[89] Y. Long and B. Zhang, Unsupervised data-driven classification of topological gapped systems with symmetries, Phys. Rev. Lett. **130**, 036601 (2023).
[90] C. Loh, T. Christensen, R. Dangovski, S. Kim, and M. Soljačić, Surrogate- and invariance-boosted contrastive learning for data-scarce applications in science, Nat. Commun. **13**, 4223 (2022).
[91] O. Khatib, S. Ren, J. Malof, and W. J. Padilla, Deep learning the electromagnetic properties of metamaterials—a comprehensive review, Adv. Funct. Mater. **31**, 2101748 (2021).
[92] R. E. Christiansen, F. Wang, O. Sigmund, and S. Stobbe, Designing photonic topological insulators with quantum-spin-Hall edge states using topology optimization, Nanophotonics **8**, 1363 (2019).
[93] A. Ghorashi, S. Vaidya, M. C. Rechtsman, W. A. Benalcazar, M. Soljačić, and T. Christensen, Prevalence of two-dimensional photonic topology: Dataset, Zenodo (2024), https://zenodo.org/records/10836524.